Eur. Phys. J. B **2**, 237–247 (1998)

THE EUROPEAN PHYSICAL JOURNAL B

Viable improvement of the full potential linearized augmented plane wave (FLAPW) method

C.P. Beulshausen and L. Fritsche[a]

Institut für Theoretische Physik der TU Clausthal, Leibnizstrasse 10, 38678 Clausthal-Zellerfeld, Germany

Received: 31 May 1997 / Revised: 12 December 1997 / Accepted: 18 December 1997

Abstract. A characteristic feature of the Full Potential Linearized Augmented Plane Wave (FLAPW)-method consists in the spatial subdivision of the charge density analogous to that of the one–particle wavefunctions, *i.e.* into a portion that is expanded in terms of spherical harmonics Y_{lm} inside the muffin–tin spheres and into a plane wave expansion of the interstitial charge density. To obtain the Hartree potential inside the spheres one is hence forced to solve a boundary value problem at the sphere surface. In addition, in all non-equivalent spheres each (l, m)-component of the charge density is mapped onto 300-400 radial grid points. To ensure an accelerated convergence of the calculation, the pertinent schemes require this rather large data set to be stored and mixed within 3–6 iteration steps. We show and illustrate for the example of a spin-polarized Ni–film with and without an oxygen overlayer and for bulk Si that this data set can be compressed by at least two orders of magnitude if one partitions the charge density in a different way so that the relevant portion determining the interatomic bonding can be Fourier expanded throughout the lattice cell. One thereby arrives at a modified FLAPW-scheme that combines favorable features of the original method with virtues of the pseudopotential method which consist in the simple construction of the Hartree potential and the efficient way of achieving self-consistency. These advantages can be exploited to the fullest by using Fast Fourier Transform. Moreover, forces that atoms experience in off-equilibrium positions attain a particularly simple form in terms of the charge density expansion coefficients.

PACS. 71.20.-b Electron density of states and band structure of crystalline solids – 71.22.+i Electronic structure of liquid metals and semiconductors and their alloys – 75.70.-i Magnetic films and multilayers

1 Introduction

The most successful method of calculating electronic ground state properties of solids on a first principles basis consists in solving the associated Kohn-Sham (KS) equations [1] upon which the original N-electron Schrödinger equation can be rigorously mapped. This is achieved by gradually reducing the electron-electron interaction and simultaneously turning on an additional external potential that finally attains the form

$$\hat{V}_{\rm ext}(\mathbf{r}, s) = V_{\rm H}(\mathbf{r}) + V_{\rm xc}(\mathbf{r}, s) \tag{1}$$

when the electron-electron interaction has been switched off completely with the constraint that the charge density is retained. (See *e.g.* [2–4].) The function $V_{\rm H}(\mathbf{r})$ denotes the Hartree potential

$$V_{\rm H}(\mathbf{r}) = \int \frac{\rho(\mathbf{r}')}{|\mathbf{r} - \mathbf{r}'|} {\rm d}^3 r' \tag{2}$$

and $V_{\rm xc}(\mathbf{r}, s)$ represents the exchange–correlation potential which is rigorously local and energy-independent. The latter reflects a fundamental conceptual difference from the self-energy expression in the quasi-particle equations that can alternatively be used to describe the solid under study, however, with a definitely different meaning of the respective quantities [5–7].

In a non-relativistic or scalar-relativistic N-electron theory, the total electronic charge density $\rho(\mathbf{r})$ can be subdivided into spin-resolved densities $\rho_s(\mathbf{r})$ so that

$$\rho(\mathbf{r}) = \sum_s \rho_s(\mathbf{r}) \tag{3}$$

and

$$N = \sum_s N_s, \tag{4}$$

where $s = \pm 1$ refers to the spin orientations. It can be shown that $V_{\rm xc}(\mathbf{r}, s)$ can be constructed for any N-electron eigenstate [8] without resorting to functional derivatives whose conformity with N-representability requirements is questionable. (See *e.g.* [9]). Ferromagnetic materials are distinct by the property that

$$N_\uparrow > N_\downarrow \, .$$

[a] e-mail: fritsche@pt.tu-clausthal.de

By construction, the densities $\rho_s(\mathbf{r})$ of the interacting system are exactly given by

$$\rho_s(\mathbf{r}) = \sum_i^{(N_s)} |\psi_{is}(\mathbf{r})|^2. \tag{5}$$

The one-particle states satisfy the KS-equations (in Hartree units)

$$\mathbb{H}\psi_{is}(\mathbf{r}) = \epsilon_{is}\psi_{is}(\mathbf{r}) \tag{6}$$

where

$$\mathbb{H} = -\frac{1}{2}\underline{\nabla}^2 + V_{\text{ext}}(\mathbf{r}) + \hat{V}_{\text{ext}}(\mathbf{r}, s) \tag{7}$$

and $V_{\text{ext}}(\mathbf{r})$ denotes the "external potential" set-up by the atomic nuclei of the solid. In some cases it may contain additional terms that relate to electrostatic fields applied from outside the solid. In a scalar-relativistic approximation the Hamiltonian $\mathbb{H}$ is slightly modified (see *e.g.* Fritsche *et al.* [10])

There is an important feature of the KS-scheme that is only little emphasized in the literature: since $\mathbb{H}$ depends on the one-particle states *via* equations (1) to (5), the KS-scheme requires high quality solutions to Eq. (6) even when one is only interested in good quality one-particle energies ϵ_{is}. As to the practical calculations of the functions $\psi_{is}(\mathbf{r})$, the Full Potential Linearized Augmented Plane Wave (FLAPW) method has emerged as one of the most accurate schemes. It was originally advanced by Andersen [11] and by Koelling and Arbman [12]. Relevant technical details were later worked out by Freeman and associates [13,14] who applied the method to solid slabs with and without overlayers. (See *e.g.* [15]). Related versions for the treatment of bulk materials were developed by Jansen and Freeman [16], Mattheiss and Hamann [17] and by Schwarz [18].

The method builds on Slater's original APW-concept which exploits the fact that the functions $\psi_{is}(\mathbf{r})$ resemble hybridized atomic orbitals within appropriately chosen, non-overlapping spheres ("muffin-tin-spheres", henceforth referred to as region I) and that they should behave nearly-free-electron-like within the flat potential interstitial region (referred to as II). The spheres around the pertinent atomic centers are usually chosen as large as possible so that they touch each other. If the aspherical variations of the potential inside the spheres are averaged out, the solutions to equation (6) can be separated into a radial and an angular dependent portion which define partial waves of certain angular momentum. Linear combinations of them can then be used to match onto individual plane waves. The augmented plane waves thus constructed form a set of basis functions in terms of which $\psi_{is}(\mathbf{r})$ is expanded. Minimization of the pertinent expectation value of $\mathbb{H}$ yields the expansion coefficients.

In the full potential version of the APW-method one forms this expectation value of $\mathbb{H}$ with the true lattice potential given by $V_{\text{ext}}(\mathbf{r}) + \hat{V}_{\text{ext}}(\mathbf{r}, s)$. It should be noted, however, that the resulting one-particle functions $\psi_{is}(\mathbf{r})$ still remain approximate solutions to equation (6): inside the spheres $\psi_{is}(\mathbf{r})$ is represented by a linear combination of partial waves whose pertinent radial components depend on the angular momentum only, but it would depend on the magnetic quantum number as well if it were to represent a partial wave of the exact solution.

Achieving self-consistency in systems with large unit cells poses quite often a technical difficulty that can seriously limit the applicability of the method. The missing row-type adsorbate/substrate systems Op(2×1)/Cu(110) and Op(2×1)/Ni(110) that have previously been studied by our group [19] constitute instructive examples of this kind. In the case of the ferromagnetically ordered Op(2×1)/Ni(110) system a standard FLAPW-calculation took more than 200 iterations to establish self-consistency. One of the sources of this shortcoming may be seen in the procedure commonly applied in mixing the information of the charge density $\rho_s(\mathbf{r})$ obtained in consecutive iteration steps. Inside the spheres this information consists of the set of density values for grid points that are used in numerically integrating the radial part of the one-particle equations. This is a very large set of several thousands of elements per atom that are mixed in a particular way with the respective elements of the preceding iterations or — in the simplest case — only with those of the immediately preceding step.

A typical phenomenon that critically influences the speed of convergence in open structures like adsorbate/substrate systems is the oscillatory bulk-surface charge transfer. These oscillations give rise to oscillations of the Hartree-potential which, in turn, drives the changes of the charge density. In the conventional scheme one mixes the grid point data on the charge density irrespective of the resulting effect on the Hartree Potential. In a Fourier expansion of the charge density (with an appropriate cut-off momentum $K_{\max}$) a charge transfer between atomic layers is reflected in a corresponding change of some Fourier components whose wavelengths are comparable to the average distance between regions of charge exchange. Since the Fourier expansion of $V_{\text{H}}(\mathbf{r})$ is given by the same coefficients $\rho_{\mathbf{K}}$ divided by $\frac{\mathbf{K}^2}{4\pi}$, a mixing of the $\rho_{\mathbf{K}}$'s from consecutive iteration steps (or from a set of steps) causes changes of the associated "Hartree-coefficients" $V_{\mathbf{K}}^{\text{H}}$ that are weighted by $\frac{1}{\mathbf{K}^2}$ so that relatively local fluctuations of $\rho_s(\mathbf{r})$ can hardly effect $V_{\text{H}}(\mathbf{r})$ or they are completely suppressed because of the cut-off imposed on the expansion.

The practical virtues of this alternative way of handling charge density data are obvious from pseudopotential calculations on comparable or identical systems which tend to converge considerably faster. The benefits of using a plane wave expansion throughout the unit cell are to some extent balanced by the requirement of appropriately pseudizing the original all-electron potential and using a considerably larger set of plane waves than is typical of an equivalent FLAPW-calculation. It is the objective of the present study to show that one can exploit the striking advantage of expanding $\rho_s(\mathbf{r})$ in terms of non-augmented *i.e.* true plane waves even when the band states are

generated within the FLAPW-scheme. We want to emphasize that our scheme is *not* aimed at changing the FLAPW-representation of the *individual* states $\psi_{is}(\mathbf{r})$ within the spheres, as distinct from various suggestions repeatedly discussed in the literature.

In Section 2 we outline how one can subdivide the valence charge density such that one portion, $\tilde{\rho_s}(\mathbf{r})$,can be kept frozen throughout the iterations and only the Fourier-expandable remainder, $\rho_s^{\mathrm{PW}}(\mathbf{r})$, undergoes changes from iteration step to iteration step. Sections 3, 4 5 deal with the associated electrostatic potentials in the two regions (I and II) and with the exchange-correlation potential. Applications are summarily discussed in Section 6. In Section 7 we particularly address results on ultrathin ferromagnetic Ni-films with and without an oxygen adlayer. Finally, in Section 8 we compare our band structure of silicon for some special points of the first Brillouin zone to that of a standard FLAPW-calculation based on the Viennese code "Wien 95" [18].

2 Subdivision of the charge density

We consider the fundamental volume V of a periodic lattice that may be subdivided into unit cells of volume Ω. For simplicity we assume the unit cell to contain one atom only. Moreover, we confine ourselves to paramagnetic systems which are uniquely characterized by the pertinent total charge density $\rho(\mathbf{r})$. In the following $\rho(\mathbf{r})$ is meant to include the contribution of the nucleus so that

$$\int_{\Omega} \rho(\mathbf{r}) \mathrm{d}^3 r = 0. \tag{8}$$

Hence, if we expand

$$\rho(\mathbf{r}) = \sum_{\substack{\mathbf{K} \\ \mathbf{K} \neq 0}}^{|\mathbf{K}_{\max}|} \rho_{\mathbf{K}} \mathrm{e}^{i\mathbf{K}\cdot\mathbf{r}} \tag{9}$$

where $\mathbf{K}$ denotes vectors of the reciprocal lattice, the term pertaining to $\mathbf{K} = 0$ may be left out. The associated electrostatic potential is then given by

$$V_{\mathrm{el}}(\mathbf{r}) = \sum_{\substack{\mathbf{K} \\ \mathbf{K} \neq 0}}^{|\mathbf{K}_{\max}|} V_{\mathbf{K}} \mathrm{e}^{i\mathbf{K}\cdot\mathbf{r}} \tag{10}$$

where

$$V_{\mathbf{K}} = 4\pi \frac{\rho_{\mathbf{K}}}{K^2} \cdot \tag{11}$$

As is evident from this simple interconnection between $V_{\mathbf{K}}$ and $\rho_{\mathbf{K}}$, a Fourier expansion offers a considerable practical advantage. On the other hand, it is clear that $\rho(\mathbf{r})$ varies so strongly within the atomic spheres that the convergence of expansion (9) is impractically slow. We therefore replace $\rho(\mathbf{r})$ inside the spheres by a considerably smoother function the choice of which is relatively obvious: We expand $\rho(\mathbf{r})$ in terms of spherical harmonics, $Y_L(\hat{\mathbf{r}})$, with respect to the center of the atom.

$$\rho(\mathbf{r}) = \sum_{L} \rho_L(\mathbf{r}) Y_L(\hat{\mathbf{r}}). \tag{12}$$

We have abbreviated the two indices l and m into L, and $\hat{\mathbf{r}}$ denotes the angle-dependent part of $\mathbf{r}$. Each of the functions $\rho_L(r)$ is now substituted by a Gaussian

$$\rho'_L(r) = a_L \mathrm{e}^{b_L r^2} \tag{13}$$

where the parameters a_L and b_L can easily be determined such that $\rho'_L(r)$ smoothly runs into $\rho_L(r)$ at the sphere surface. Hence, the function

$$\rho'(\mathbf{r}) = \begin{cases} \sum\limits_{L} \rho'_L(r) Y_L(\hat{\mathbf{r}}) & \text{if } \mathbf{r} \text{ is in region I} \\ \sum\limits_{\mathbf{K}} \rho_{\mathbf{K}} \mathrm{e}^{i\mathbf{K}\cdot\mathbf{r}} & \text{if } \mathbf{r} \text{ is in region II} \end{cases} \tag{14}$$

represents a portion of the total charge density whose plane wave expansion may be expected, and proves to be, relatively fast convergent. However, if one were to use this definition of $\rho'(\mathbf{r})$ at each iteration step, the remaining charge densities inside the spheres would change similarly to the original one, and one could not avoid mixing grid point data contrary to our intention. We therefore use the definitions (13), (14) for $\rho'(\mathbf{r})$ only after the first iteration step and introduce a difference charge density, $\tilde{\rho}_1(\mathbf{r})$, by setting

$$\tilde{\rho}_1(\mathbf{r}) = \rho_1(\mathbf{r}) - \rho'_1(\mathbf{r}) \tag{15}$$

where $\rho_1(\mathbf{r})$ is the total charge density obtained within that step, and we now keep $\tilde{\rho}_1(\mathbf{r})$ frozen in the ensuing calculations. In certain cases where one wants to achieve higher accuracy, it might be necessary to replace $\tilde{\rho}_1(\mathbf{r})$ once in a while by a relaxed, analogously constructed charge density $\tilde{\rho}_\nu(\mathbf{r})$ after the ν-iteration step. By construction $\tilde{\rho}_1(\mathbf{r})$ vanishes smoothly at the sphere surface and remains zero outside. Hence, if one defines for any further iteration step

$$\rho^{\mathrm{PW}}(\mathbf{r}) = \begin{cases} \rho(\mathbf{r}) - \tilde{\rho}_1(\mathbf{r}) & \text{if } \mathbf{r} \text{ is in region I} \\ \sum\limits_{\mathbf{K}} \rho_{\mathbf{K}} \mathrm{e}^{i\mathbf{K}\cdot\mathbf{r}} & \text{if } \mathbf{r} \text{ is in region II} \end{cases} \tag{16}$$

where $\rho_{\mathbf{K}}$ is obtained as before by summing over the APW-contributions and $\rho(\mathbf{r})$ denotes the total charge density obtained in that step, $\rho^{\mathrm{PW}}(\mathbf{r})$ is a smooth function everywhere and can be expanded in a relatively fast converging Fourier series

$$\rho^{\mathrm{PW}}(\mathbf{r}) = \sum_{\mathbf{K}}^{|\mathbf{K}_{\max}|} \rho_{\mathbf{K}}^{\mathrm{PW}} \mathrm{e}^{i\mathbf{K}\cdot\mathbf{r}} \,. \tag{17}$$

The way we have constructed $\rho^{\mathrm{PW}}(\mathbf{r})$ bears a strong resemblance to the concept of pseudo-charge density as has been proposed by Weinert [20] and has become a crucial element of the original FLAPW method. Both types of pseudo-charge densities guarantee optimal convergence

in Fourier space and smoothness at the sphere boundary. However, within our scheme the total charge density is given by

$$\rho(\mathbf{r}) = \tilde{\rho}_1(\mathbf{r}) + \rho^{\mathrm{PW}}(\mathbf{r})$$

and is hence completely determined by $\rho^{\mathrm{PW}}(\mathbf{r})$ at each iteration step as $\tilde{\rho}_1(\mathbf{r})$ is kept frozen. This is distinctly different from Weinert's construction of $\rho(\mathbf{r})$ where a similar subdivision is used but neither of the charge densities on the right-hand side is kept fixed and therefore each term contributes to the changes of the total charge density as one runs through the iterations. Since our method connects the changes of $\rho(\mathbf{r})$ uniquely to those of $\rho^{\mathrm{PW}}(\mathbf{r})$, any procedure used to accelerate convergence now involves only the associated Fourier coefficients.

3 Electrostatic potential in the interstitial region

Except for a small truncation error in equation (17) which is kept below a practical threshold of accuracy by choosing $|\mathbf{K}_{\max}|$ sufficiently large, $\rho^{\mathrm{PW}}(\mathbf{r})$ is identical with the true charge density $\rho(\mathbf{r})$ in region II. The electrostatic potential, $V_{\mathrm{el}}(\mathbf{r})$, in this region depends, however, on the sphere charge density $\tilde{\rho}_1(\mathbf{r})+\rho^{\mathrm{PW}}(\mathbf{r})$ as well. By definition $\tilde{\rho}_1(\mathbf{r})$ contains a large monopole portion, $\tilde{\rho}_{10}(\mathbf{r})$, and multipole components for $l > 0$. The latter contributions to $V_{\mathrm{el}}(\mathbf{r})$ will be shown to be negligibly small. The monopole component arises from the centro-symmetric electronic charge density, $\tilde{\rho}^{\mathrm{el}}_{10}(\mathbf{r})$, contained in $\tilde{\rho}_{10}(\mathbf{r})$ and from the nuclear charge density $-Z\delta(\mathbf{r})$. We denote the charge in the sphere, associated with $\tilde{\rho}_{10}(\mathbf{r})$ by $\tilde{Q}_{\mathrm{Ion}}$, which is given by

$$\tilde{Q}_{\mathrm{Ion}} = -Z + \int_{\Omega_I} \tilde{\rho}^{\mathrm{el}}_{10}(\mathbf{r})\mathrm{d}^3r$$

and describes the charge not contained in the Fourier expandable portion $\rho^{\mathrm{PW}}(\mathbf{r})$. The spatial variation of $V_{\mathrm{el}}(\mathbf{r})$ in region II remains to an adjustable degree of accuracy unaffected by replacing $\tilde{\rho}_{10}(\mathbf{r})$, for example, with a Gaussian

$$\rho'_{\mathrm{Ion}}(r) = \tilde{Q}_{\mathrm{Ion}}\mathrm{e}^{-\left(\frac{r}{\lambda}\right)^2}/(\sqrt{\pi}\lambda)^3 \tag{18}$$

where λ is defined by requiring

$$4\pi\int_0^{R_{\mathrm{sph}}} \rho'_{\mathrm{Ion}}(r)r^2\mathrm{d}r = \tilde{Q}_{\mathrm{Ion}}(1-\gamma)$$

with R_{sph} denoting the sphere radius. A Gaussian offers the advantage of fastest convergence in Fourier space. The relative charge error, γ, can be adjusted to practical accuracy requirements and was chosen to be of the order 10^{-3}. In the following we shall ignore the finiteness of this error. Hence the charge density

$$\rho^{\mathrm{PW}}_{\mathrm{Ion}}(\mathbf{r}) = \rho^{\mathrm{PW}}(\mathbf{r}) + \rho'_{\mathrm{Ion}}(\mathbf{r}) \tag{19}$$

yields zero charge when integrated over the entire unit cell so that the electrostatic potential in region II can be expressed as

$$V^{\mathrm{II}}_{\mathrm{el}}(\mathbf{r}) = \sum_{\substack{\mathbf{K}\\ \mathbf{K}\neq 0}}^{|\mathbf{K}_{\max}|} V_{\mathbf{K}}\mathrm{e}^{i\mathbf{K}\cdot\mathbf{r}} \tag{20}$$

where

$$V_{\mathbf{K}} = 4\pi\frac{\rho^{\mathrm{PW}}_{\mathbf{K}} + \rho'^{\mathrm{Ion}}_{\mathbf{K}}}{K^2}\ . \tag{21}$$

The quantities $\rho^{\mathrm{PW}}_{\mathbf{K}}$ and $\rho'^{\mathrm{Ion}}_{\mathbf{K}}$ denote Fourier coefficients of $\rho^{\mathrm{PW}}(\mathbf{r})$ and $\rho'_{\mathrm{Ion}}(\mathbf{r})$, respectively.

We temporarily consider the plane wave expansion of $\rho^{\mathrm{PW}}(\mathbf{r})$ in II being continued into the spherical region and expanded according to equation (12) with the radial components denoted by $\rho^{\mathrm{PW}}_L(r)$. We may express the aspherical components of $\tilde{\rho}_1(\mathbf{r})$ for $l > 0$ as

$$\tilde{\rho}_{1L}(\mathbf{r}) = \left[\rho'_{1L}(\mathbf{r}) - \rho^{\mathrm{PW}}_{1L}(\mathbf{r})\right] Y_L(\hat{\mathbf{r}})\ . \tag{22}$$

Their contribution to $V^{\mathrm{II}}_{\mathrm{el}}(\mathbf{r})$ is negligibly small for the following reason. If one replaces the bracketed term on the right-hand side by a first order Taylor polynomial referenced to the sphere radius, this function of $\mathbf{r}$ vanishes identically due to our requirement that $\rho'_{1L}(\mathbf{r})$ be a smooth continuation of $\rho^{\mathrm{PW}}_{1L}(r)$ inside the sphere. As one moves away from the sphere surface towards the center non-linear terms of the Taylor expansion become sizable, but the weight r^{l+2} in the definition of the multipole moment q_L of $\tilde{\rho}_1(\mathbf{r})$, *viz.*

$$q_L = \int_0^{R_{\mathrm{sph}}} \left[\rho'_{1L}(\mathbf{r}) - \rho^{\mathrm{PW}}_{1L}(\mathbf{r})\right] r^{l+2}\mathrm{d}r$$

decreases correspondingly so that the integral yields always zero on the scale of interest, which has routinely been checked in our calculations. As the accuracy of the original FLAPW-method is tightly connected to the accuracy with which one recovers the true multipole moments by using appropriate pseudo-charge densities, the above result states that our method ensures comparable accuracy.

We could have defined $\tilde{\rho}_1(\mathbf{r})$ alternatively by equating this function only to the spherical difference charge density, *i.e.* to $\tilde{\rho}_{1L}(\mathbf{r})$ in equation (22) for $l = 0$. According to equation (16) the entire aspherical variation of the total charge density inside the sphere is then absorbed into $\rho^{\mathrm{PW}}(\mathbf{r})$ which results in a slower convergence of the Fourier expansion (17). Quite often, this constitutes only a minor drawback and is compensated by simplifications in other places. The multipole components of the charge density are quantitatively contained then in the plane wave expansion of $\rho^{\mathrm{PW}}(\mathbf{r})$, in complete analogy to the pseudopotential method which requires, however, considerably more plane waves. The latter is a consequence of the fact that pseudization of the original potential leads to a smoothing of the radial dependence of the charge density

that is much less effective than our procedure of forming $\rho^{\mathrm{PW}}(\mathbf{r})$ by subtracting $\tilde{\rho}_{1L}(\mathbf{r})$ for $l = 0$.

In practically determining the Fourier coefficients $\rho^{\mathrm{PW}}_{\mathbf{K}}$ we use a Fast Fourier Transform (FFT) algorithm which requires a three-dimensional lattice of grid points within the unit cell. The number of these points is determined by $|\mathbf{K}_{\max}|$.

4 Electrostatic potential within the spherical region and forces

Since $\tilde{\rho}_1(\mathbf{r}) - \rho'_{\mathrm{Ion}}(\mathbf{r})$ possesses a zero monopole component, vanishes smoothly at the sphere surface and remains zero in the interstitial region, the real-space integration for the potential

$$V'_{\mathrm{el}}(\mathbf{r}) = \int_V \frac{\tilde{\rho}_1(\mathbf{r}') - \rho'_{\mathrm{Ion}}(\mathbf{r}')}{|\mathbf{r}' - \mathbf{r}|} \mathrm{d}^3 r' \tag{23}$$

may be confined to the Ω_{I}-portions of V. If one casts $V^{\mathrm{II}}_{\mathrm{el}}(\mathbf{r})$, given by equation (20), as a Poisson integral

$$V^{\mathrm{II}}_{\mathrm{el}}(\mathbf{r}) = \int_V \frac{\rho^{\mathrm{PW}}(\mathbf{r}') + \rho'_{\mathrm{Ion}}(\mathbf{r}')}{|\mathbf{r}' - \mathbf{r}|} \mathrm{d}^3 r'$$

and forms

$$V_{\mathrm{el}}(\mathbf{r}) = V'_{\mathrm{el}}(\mathbf{r}) + V^{\mathrm{II}}_{\mathrm{el}}(\mathbf{r}) \tag{24}$$

one recognizes that in region II $V_{\mathrm{el}}(\mathbf{r})$ is identical with $V^{\mathrm{II}}_{\mathrm{el}}(\mathbf{r})$, *i.e.* with the true electrostatic potential, and it becomes also identical with the true electrostatic potential in region I because of

$$[\tilde{\rho}_1(\mathbf{r}) - \rho'_{\mathrm{Ion}}(\mathbf{r})] + \left[\rho^{\mathrm{PW}}(\mathbf{r}) + \rho'_{\mathrm{Ion}}(\mathbf{r})\right] = \rho(\mathbf{r})$$

which follows from our definition (16). It should be emphasized that in determining $V_{\mathrm{el}}(\mathbf{r})$ according to equation (24) one does not have to solve a boundary value problem at the sphere surface, different from the standard FLAPW-method [14]. Furthermore, in applying the FLAPW-method one customarily expands $V_{\mathrm{el}}(\mathbf{r})$ in the form

$$V_{\mathrm{el}}(\mathbf{r}) = \begin{cases} \sum\limits_L V_L(r) Y_L(\hat{\mathbf{r}}) & \text{if } \mathbf{r} \text{ is in region I} \\ \sum\limits_{\mathbf{K}} V_{\mathbf{K}} \mathrm{e}^{i\mathbf{K}\cdot\mathbf{r}} & \text{if } \mathbf{r} \text{ is in region II.} \end{cases} \tag{25}$$

If we use our subdivision (24) we may cast $V_L(r)$ as

$$V_L(\mathbf{r}) = V'_L(\mathbf{r}) + V^{\mathrm{II}}_L(\mathbf{r}) \; .$$

In the FLAPW-form of the Hamiltonian matrix that defines the general eigenvalue problem to be solved in order to obtain the band structure, $V_{\mathrm{el}}(\mathbf{r})$ is mapped onto matrix elements

$$V_{\mathbf{K}'\mathbf{K}} = V^{\mathrm{I}}_{\mathbf{K}'\mathbf{K}} + V^{\mathrm{II}}_{\mathbf{K}'\mathbf{K}} \tag{26}$$

where the two terms on the right refer to integrals that are taken over the respective regions. The second term has the form

$$V^{\mathrm{II}}_{\mathbf{K}'\mathbf{K}} = \int_{\Omega_{\mathrm{II}}} V_{\mathrm{el}}(\mathbf{r}) \mathrm{e}^{i(\mathbf{K}-\mathbf{K}')\cdot\mathbf{r}} \mathrm{d}^3 r \tag{27}$$

where $V_{\mathrm{el}}(\mathbf{r}) = V^{\mathrm{II}}_{\mathrm{el}}(\mathbf{r})$ may be expressed by expansion (20). The contribution $V^{\mathrm{I}}_{\mathbf{K}'\mathbf{K}}$ is calculated by using the augmentations of the respective plane waves and by employing the angular momentum decomposition of $V_{\mathrm{el}}(\mathbf{r})$. It is possible, however, to avoid the subdivision (26) of $V_{\mathbf{K}'\mathbf{K}}$ by exploiting the following properties of the APW's and $V_{\mathrm{el}}(\mathbf{r})$. As distinct from Slater's original idea, each plane wave in the FLAPW-method is augmented by matching it *smoothly* onto a partial wave expansion inside the sphere. Hence the plane wave is still well approximated by the partial wave expansion within a certain shell below the sphere surface. Aspherical variations of $V_{\mathrm{el}}(\mathbf{r})$ associated with $V_L(r)$ for $l > 0$ are usually large only within that shell and rapidly decay farther into the sphere. On the other hand, these aspherical components of $V_{\mathrm{el}}(\mathbf{r})$ are also well approximated by the plane wave expansion in equation (25) if one extends its range of validity into that shell region. To a rather good approximation one can therefore determine $V_{\mathbf{K}'\mathbf{K}}$ by forming an integral such as in equation (27) but with Ω substituted for Ω_{II}. One has to observe, however, that the spherical component of $V_{\mathrm{el}}(\mathbf{r})$, *i.e.* $V_0(\mathbf{r})$, yields a contribution to $V_{\mathbf{K}'\mathbf{K}}$ that can only be calculated by using the augmentations of the plane waves and forming an integral of the type $V^{\mathrm{I}}_{\mathbf{K}'\mathbf{K}}$. This would, of course, also contain $V^{\mathrm{II}}_0(\mathbf{r})$, as is evident from equation (24). But since this contribution occurs automatically in the second integral of equation (26) when taken over the entire cell, one must confine the spherical component of $V_{\mathrm{el}}(\mathbf{r})$ in $V^{\mathrm{I}}_{\mathbf{K}'\mathbf{K}}$ to $V'_0(\mathbf{r})$ only.

If one uses the alternative definition of $\tilde{\rho}_1(\mathbf{r})$ by equating this function to $\tilde{\rho}_{1L}(\mathbf{r})$ in equation (22) for $l = 0$, it turns out that the forces acting on the atoms in the unit cell can be expressed in a particularly simple form. One obtains

$$\mathbf{F}_\alpha = -\sum_{\mathbf{K}} i\mathbf{K} \frac{\rho^{\mathrm{PW}}_{\mathbf{K}}}{K^2} \mathrm{e}^{i\mathbf{K}\cdot\mathbf{R}_\alpha}$$

where $\mathbf{F}_\alpha$ denotes the force on the α-th atom having the position $\mathbf{R}_\alpha$ in the unit cell. The derivation of this equation will be published elsewhere.

5 The exchange-correlation potential

We have used the exchange-correlation potential suggested by Barth and Hedin [21] throughout our calculations to alleviate a comparison with earlier calculations. An implementation of more advanced versions including gradient corrections does, of course, not pose any difficulty. In any case, $V_{\mathrm{xc}}(\mathbf{r})$ in terms of its Fourier expansion

$$V_{\mathrm{xc}}(\mathbf{r}) = \sum_{\mathbf{K}} v_{\mathrm{xc}}(\mathbf{K}) \mathrm{e}^{i\mathbf{K}\cdot\mathbf{r}} \; ,$$

can be obtained from $\rho^{\mathrm{PW}}(\mathbf{r})$ by calculating $V_{\mathrm{xc}}(\mathbf{r})$ in Ω grid point by grid point and subsequently performing a Fast Fourier Transform. This expansion holds for the interstitial region. Within the spheres one forms $V_{\mathrm{xc}}(\mathbf{r})$ from $\rho(\mathbf{r})$ according to equation (16) and expands

$$V_{\mathrm{xc}}(\mathbf{r}) = \sum_L v_{\mathrm{xc}}(L,r) Y_L(\hat{\mathbf{r}}) \; .$$

6 Applications

To demonstrate the functioning of our new FLAPW-version we have first carried out calculations on fcc-bulk copper and ferromagnetically ordered fcc-nickel metal and obtained complete agreement with the respective standard FLAPW-results. In assessing the accuracy of our results we have compared the respective band structures, total and angular momentum decomposed densities of states, effective orbital occupation numbers and magnetic moments per atom. The agreement proved to be within the range of numerical errors that are typical of high quality band structure methods. We have extended then our calculations to unsupported 3-layer (100)-films of Cu and Ni metal with and without p(1×1) oxygen overlayers. To this purpose, we have modified our computer code by using the concept of repeated slabs. Thereby one gains the advantage that the vacuum region between the slabs can be treated as an extension of the interstitial region so that one avoids solving an extra boundary value problem at the planes confining the slab towards the vacuum. The latter is a typical feature of the FLAPW-single-slab-method. Ferromagnetically ordered Op(1×1)-Ni(100) films represent particularly critical systems with a rather fragile stability of convergence. This will be the subject of Section 7. We have, furthermore, tested our new method by calculating the electronic structure of the alkali halides, the solid rare gases and the prototype semiconductors GaAs and Si. Results on the latter material will shortly be discussed in Section 8. In Table 1 we have listed the various bulk and slab-materials, respectively, that have successfully been studied by using our new scheme.

Table 1. List of materials that have been treated within the modified FLAPW-scheme.

Material	Structure	Spin order
Ni	fcc - bulk	ferromagn.
Cu		paramagn.
Ne		paramagn.
Ar		paramagn.
Kr		paramagn.
Si	diamond	paramagn.
GaAs	zincblende	
NaCl	fcc-based unit cell	paramagn.
NaF		
KCl		
LiF		
Cu	1-layer (100) film	paramagn.
Cu	3-layer (100) film	
Ni	1-layer (100) film	
Ni	3-layer (100) film	ferromagn.
Ni	6-layer (100) film	
Cu	3-layer (100) film of Cu with Op(1×1)	paramagn.
Ni	3-layer (100) film of Ni with Op(1×1)	ferromagn.

Table 2. Average number of valence electrons in the interstitial region and inside the muffin-tin-spheres for a Ni(100)-film with an O-adlayer for 4 different distances $d_{\mathrm{O-Ni}}$. The corresponding data for bulk Ni, for the uncovered 6-layer Ni-film (this work) and for a 7-layer Ni-film (Wimmer *et al.* [25]) are also given.

$\mathrm{Ni}^{(3)}$	$\mathrm{Ni}^{(2)}$	$\mathrm{Ni}^{(1)}$)		interstitial region	
9.20				0.80	bulk
9.21	9.21	9.03		ca. 4.95	7-layer film
9.19	9.23	9.04		5.01	6-layer film
$\mathrm{Ni}^{(3)}$	$\mathrm{Ni}^{(2)}$	$\mathrm{Ni}^{(1)}$	O	interstitial region	$d_{\mathrm{O-Ni}}$
9.08	9.26	9.32	3.94	4.39	1.7 a.u.
9.04	9.28	9.26	4.21	4.22	1.8 a.u.
9.08	9.23	9.24	4.33	4.11	1.9 a.u.
9.06	9.26	9.19	4.77	3.71	2.2 a.u.

7 The Op(1×1) - Ni(100) system

Among the ferromagnetic elemental metals Ni plays an exceptional role because of its large density of states (DOS) in the minority spin system at the Fermi level. This is also reflected in its very delicate behavior in establishing self-consistency, notably in slab calculations where the presence of surfaces gives rise to bulk-surface charge transfer oscillations as already mentioned earlier. Oxygen in contact with Ni undergoes strong covalent bonding which conflicts with the persistence of ferromagnetic order. Hence, a slab-calculation on a Ni-film with and without an oxygen overlayer constitutes a particular sensitive test case for our new scheme. We have chosen a Ni(100)-rather than a Ni(111)-film because of the simpler symmetry and for reasons of comparability with an already existing calculation by Godby *et al.* [22,23] on the Op(1×1)-Ni(100) system. However, ferromagnetic spin order was not taken into account by these authors.

As indicated by the results of Godby *et al.* [22,23], an Op(1×1) overlayer on Ni(100) can actually not be formed in reality because of the considerable interatomic repulsion between the oxygen atoms. At sufficiently low coverage one only observes an initial formation of a $p(2 \times 2)$ array of oxygen which transforms into $c(2 \times 2)$ array. Beyond half coverage the system starts forming NiO [24]. Notwithstanding the actual instability of the Op(1×1)/Ni(100) system it can well serve as a particularly sensitive testing ground for our new scheme. We have first performed a self-consistent calculation on a 6-layer unreconstructed Ni film without an overlayer. In using a repeated slab method, one

Table 3. Angular momentum decomposed charges in the muffin-tin spheres. The data refer to the same calculations as Table 2.

s-charge				p-charge				d-charge				
$Ni^{(3)}$	$Ni^{(2)}$	$Ni^{(1)}$		$Ni^{(3)}$	$Ni^{(2)}$	$Ni^{(1)}$		$Ni^{(3)}$	$Ni^{(2)}$	$Ni^{(1)}$		
0.42				0.45				8.3				bulk
0.45	0.45	0.43		0.43	0.43	0.29		8.29	8.28	8.29		7-layer
0.47	0.47	0.44		0.46	0.46	0.30		8.22	8.25	8.27		6-layer
$Ni^{(3)}$	$Ni^{(2)}$	$Ni^{(1)}$	O	$Ni^{(3)}$	$Ni^{(2)}$	$Ni^{(1)}$	O	$Ni^{(3)}$	$Ni^{(2)}$	$Ni^{(1)}$	O	d_{O-Ni}
0.43	0.45	0.42	1.42	0.28	0.42	0.54	2.51	8.34	8.35	8.23	0.01	1.7
0.43	0.45	0.40	1.48	0.28	0.41	0.51	2.72	8.31	8.34	8.21	0.01	1.8
0.43	0.46	0.40	1.51	0.28	0.42	0.51	2.80	8.34	8.31	8.22	0.01	1.9
0.43	0.46	0.39	1.63	0.27	0.42	0.44	3.10	8.33	8.35	8.28	0.01	2.2

does not gain an advantage by confining the slab to an odd number of atomic layers, different from the standard FLAPW-single slab method. The results provide an interesting comparison with a 7-layer single slab calculation of Wimmer *et al.* [25]. We have repeated then the calculation for a 3-layer Ni-film with a $p(1\times1)$ oxygen overlayer on top and chosen the internuclear O-Ni distance, d_{O-Ni}, to be 1.7, 1.8, 1.9 and 2.2 Bohr radii, respectively. The lateral array of the oxygens was assumed to be pseudomorphic with respect to the substrate.

In Tables 2 and 3 we have compiled all data of interest for the four values of d_{O-Ni}, the smallest one being the experimental equilibrium distance for a $c(2\times2)$ overlayer (Demuth *et al.* [26]). In comparing respectively the, 6- and 7- layer film of Ni with an oxygen covered Ni-film of three layers we are counting the Ni-layers in consecutive order from the top. Obviously, there is practically no difference in the valence charges of the first three layers between our 6-layer and the 7-layer film of Wimmer *et al.* [25]. As compared to the bulk, a Ni-atom in the $Ni^{(2)}$-layer sees an unmodified environment of nearest neighbors. Not surprisingly, its charge is hardly changed. The top-layer $Ni^{(1)}$ contains slightly less charge, and this remains true also for $Ni^{(3)}$ adjacent to the vacuum in the oxygen covered film of 3 Ni-layers. Hence, the bonding effect of the oxygen film is exceedingly short-range. This loss of charge is mainly connected to a reduction of p-charge and can in tight-binding parlance be related to a reduction of nearest neighbors at the surface. As a result, the number of hopping-integrals is reduced which causes the width of the d-type structures in the local density of states (LDOS) to shrink. On the other hand, the width of this structure can alternatively be traced back to the occurrence of p-d-hybridization within the Ni-sphere. Hence a loss of p-charge goes hand in hand with a narrowing of the d-derived structure in the LDOS. As can be seen from Table 3, the s-, p- and d-charges of the 6-layer and 7-layer film for corresponding layers agree quite well. There is only a minor difference in that our d-charges vary slightly across the layers whereas the respective charges in the study of Wimmer *et al.* [25] are practically constant.

As can be seen from Table 3, the s- and p-component of the valence charge density in the oxygen layer increases as one moves this layer away. At the same time the p-charge density of the adjacent Ni-layer decreases. Moreover, the interstitial charge density drops as the oxygen charge increases (not listed).

7.1 Magnetic moments

In Table 4 we have compiled spin resolved and angular momentum decomposed occupation numbers (per muffin-tin-sphere) that result from the occupied valence bands. The difference between these occupation numbers for spin-up and spin-down, multiplied by the Bohr magneton, gives the associated magnetic moment which we have also listed. Expectedly, the d-components give by far the largest contribution to the total moment. The s- and p-components are only minute and give rise to a negative contribution. Since the pertinent partial waves are not completely localized within the muffin-tin-spheres (as opposed to the d-waves), one observes a negative magnetization in the interstitial region. The $Ni^{(3)}$-layer of the 6-layer film exhibits a magnetic moment of $0.59\mu_B$ which is again in very good agreement with the moment in bulk Ni, *viz.* $0.58\mu_B$, as obtained by using the same calculational method. The corresponding values for layers given by Wimmer *et al.* [25] are by some $10^{-2}\mu_B$ larger. Differences of this magnitude reflect quantum size effects and occur typically with films of only few atomic layers if one increases the thickness by one or two layers (*e.g.* Weimert *et al.* [19])

Experiments indicate a small surface-enhancement of the magnetic moment by about 5% which is in agreement with the trends common to such calculations on thin films. The short-range effect of the oxygen bonding is also reflected in the minute change of the magnetic moment of the $Ni^{(3)}$-layer on the other side of the film, *i.e.* the vacuum side. Only at an oxygen distance of 1.7 a.u. the moment of this layer drops slightly to $0.56\mu_B$, otherwise it is practically identical to the value without oxygen coverage. By contrast, the moment of the $Ni^{(2)}$-layer is noticeably smaller with an oxygen layer on top compared to the situation without coverage. Even at an oxygen distance of 1.8 a.u. the moment is at $0.48\mu_B$ and hence still depressed.

Table 4. Angular momentum decomposed occupation numbers $n_l^{\uparrow/\downarrow}$, moments μ_l, total magnetic moments μ, total and spin-resolved valence charges Q per atom (muffin-tin-sphere) and in the interstitial region.

Op(1 × 1)/Ni(100), 3-layer Ni substrate, $d_{\mathrm{O-Ni}} = 1.7$a.u.										
	$Ni^{(3)}$		$Ni^{(2)}$		$Ni^{(1)}$		O		interstitial region	
	$n_l^{\uparrow}$	$n_l^{\downarrow}$	$n_l^{\uparrow}$	$n_l^{\downarrow}$	$n_l^{\uparrow}$	$n_l^{\downarrow}$	$n_l^{\uparrow}$	$n_l^{\downarrow}$	$n_l^{\uparrow}$	$n_l^{\downarrow}$
s	0.22	0.22	0.22	0.22	0.21	0.21	0.71	0.71		
μ_{s}	0.0		0.0		0.0		0.0			
p	0.14	0.15	0.20	0.21	0.27	0.27	1.25	1.26		
μ_{p}	−0.01		−0.01		0.0		−0.01			
d	4.45	3.89	4.39	3.96	4.16	4.07	0.005	0.005		
μ_{d}	0.56		0.43		0.09		0.0			
$Q:\uparrow/\downarrow$	4.82	4.26	4.84	4.42	4.70	4.61	1.96	1.97	2.18	2.21
Q	9.08		9.26		9.32		3.94		4.39	
μ	0.56		0.42		0.09		−0.01		−0.03	

Ni 6-layer-film								
	$Ni^{(1)}$		$Ni^{(2)}$		$Ni^{(3)}$		interstitial region	
	$n_l^{\uparrow}$	$n_l^{\downarrow}$	$n_l^{\uparrow}$	$n_l^{\downarrow}$	$n_l^{\uparrow}$	$n_l^{\downarrow}$	$n_l^{\uparrow}$	$n_l^{\downarrow}$
s	0.219	0.221	0.235	0.238	0.235	0.238		
μ_{s}	−0.002		−0.003		−0.003			
p	0.145	0.155	0.223	0.236	0.223	0.237		
μ_{p}	−0.01		−0.013		−0.014			
d	4.46	3.82	4.43	3.83	4.41	3.80		
μ_{d}	0.64		0.60		0.61			
$Q:\uparrow/\downarrow$	4.83	4.20	4.91	4.32	4.89	4.30	1.24	1.27
Q	9.04		9.23		9.19		2.51	
μ	0.63		0.586		0.592		−0.03	

Ni 7-layer-film (Wimmer *et al.* [25])								
	$Ni^{(1)}$		$Ni^{(2)}$		$Ni^{(3)}$		interstitial region	
	$n_l^{\uparrow}$	$n_l^{\downarrow}$	$n_l^{\uparrow}$	$n_l^{\downarrow}$	$n_l^{\uparrow}$	$n_l^{\downarrow}$	$n_l^{\uparrow}$	$n_l^{\downarrow}$
s	0.21	0.22	0.22	0.23	0.22	0.23		
μ_s	−0.01		−0.01		−0.01			
p	0.14	0.15	0.21	0.22	0.21	0.22		
μ_p	−0.01		−0.01		−0.01			
d	4.50	3.79	4.46	3.82	4.46	3.83		
μ_d	0.71		0.64		0.63			
$Q:\uparrow/\downarrow$	4.85	4.16	4.89	4.27	4.89	4.28	1.18	1.23
Q	9.04		9.20		9.21		2.41	
μ	0.70		0.62		0.61		−0.05	

bulk Ni									
	s	μ_{s}	p	μ_{p}	d	μ_{d}	$Q:\uparrow/\downarrow$	Q	μ
$n_l^{\uparrow}$	0.22	0.00	0.22	−0.02	4.45	0.60	4.89	9.20	0.58
$n_l^{\downarrow}$	0.22		0.24		3.85		4.31		

Table 5. Number of iteration steps for various calculations

System	Number of iterations
O/Ni(100), Ni-substrate of 3 layers, $d_{\mathrm{O-Ni}} = 1.7$ a.u.	50
Ni(100)-film of 6 layers (this work)	30
Ni(100)-film of 7 layers (Wimmer *et al.* [25])	50
Ni fcc-bulk (this work)	14

Not surprisingly, the $Ni^{(1)}$-layer exhibits a drastical dependence of its magnetic moment on the oxygen distance d_{O-Ni}. At a distance of 1.7 a.u. one observes only a remainder of $0.09\mu_B$, that is, the moment has practically disappeared. By increasing the distance in steps of only 0.1 a.u. the moment raises to $0.3\mu_B$ and $0.38\mu_B$, respectively. At a distance of 2.2 a.u. it has become as large as $0.61\mu_B$ which exceeds even the value of the clean surface layer.

7.2 Local density of states

Distinctly different from the individual states in multilayer films whose decay length quite often extends over several layers if they are surface states, chemical bonding, as reflected in the charge density changes of the pertinent atoms, is a short-range phenomenon. This has already been pointed out earlier at various places. The local density of states (LDOS) provides another tool for discussing features of interatomic bonding. This is illustrated in Figures 1a-d where we show the spin-resolved LDOS of the $Op(1 \times 1)/Ni(100)$ system with a,b,c and d referring to the oxygen layer and the top, second and third Ni-layer, respectively. We have chosen to present the results for an O-layer distance of 1.7 a.u. which appears to be the most plausible distance as already explained earlier. The $Ni^{(3)}$-layer is facing the vacuum, as before. Its LDOS is practically identical to that of the corresponding $Ni^{(1)}$-layer in an uncovered Ni 6-layer film. One recognizes the sizable difference in the occupation for spin-up and spin-down states. (The Fermi-level is indicated by a vertical dotted line.) The adjacent $Ni^{(2)}$-layer shows hardly any change as to these principal features of the LDOS. The $Ni^{(1)}$-layer, however, which is directly involved in the O-Ni bonding displays striking differences in its LDOS, the most obvious feature being that the very close one-to-one correspondence of the structures in the spin-up and spin-down LDOS is reduced to a mere similarity and that there now additional structures in the energy regime ranging from -8 eV to -4 eV which are oxygen induced. The latter follows from inspection of Figure 1a which refers to the oxygen layer.

It is also evident from this figure that there are Ni-induced structures in the LDOS of oxygen which extend from -4 eV to $+2$ eV. This mutual interchange of characteristic structures is indicative of chemical bonding and provides a measure of estimate for the strength of the bonding. As one increases d_{O-Ni}, the widths of the O-derived and Ni-derived structures shrink and the amplitudes of the induced portions drop. At the same time the $Ni^{(1)}$-layer starts building up the spin-up/spin-down asymmetry.

7.3 Synopsis of the results

The details of the O-Ni interaction studied with our $Op(1 \times 1)/Ni(100)$-system reflect obviously general features of the O-Ni-bonding, in particular its effect on the ferromagnetic order in the nearest-neighbor Ni-atom. There is every reason to expect this effect to occur as well with the $Op(2 \times 2)/Ni(111)$ system. Since we have found with our system that one loses at the peak of the effect an equivalent of 1.5 bulk magnetic moments per oxygen atom, it is likely that the effect is much larger in the case of $Op(2 \times 2)$-overlayers where one has four surface Ni-atoms per O-adatom. Elmers and Gradmann [27] find, in fact, in their experiments on the $Op(2 \times 2)/Ni(111)$-system, that oxygen reduces the magnetic moment of this system by an equivalent of four bulk moments per oxygen adatom which strongly supports our conclusion.

7.4 Convergence of the new method

As discussed in Section 1, the primary goal of our FLAPW-version was to speed up its convergence. We have again chosen ferromagnetically ordered Ni metal and a multilayer Ni-film with and without an O-overlayer to demonstrate what can be gained by using our scheme. Because of the exceptionally high density of states in the minority spin system, calculations on those films are notorious for their fragile stability of convergence. In Table 5 we have listed for various systems the number of iteration steps that were necessary to achieve self-consistency within a threshold energy of ~ 0.1 meV for a selected number of particularly sensitive bands at special points of the Brillouin zone. Our result for the 6-layer Ni-film lends itself to a comparison with calculations by Wimmer *et al.* [25] on the 7-layer Ni-film. As distinct from our calculations that are based on a simple scheme of mixing data only of consecutive steps, these authors used an Anderson algorithm to speed up the convergence. For this reason the ratio of 30 *versus* 50 iterations lends credence to our claim that the modified FLAPW-version offers considerable practical advantages.

8 Band structure of silicon

We have compared our results to those obtained by using the WIEN 95-code [18] based on the standard FLAPW-method. We limit ourselves to comparing the respective band structures at three symmetry points Γ, X and L. The results are compiled in Table 6 where we have also listed band corrections that are due to aspherical variations of the self-consistent potential inside the spheres. If we denote this deviation of the true potential from its spherical average by $V_{\mathrm{asphr.}}(\mathbf{r})$, we can partition the Hamiltonian

$$\mathsf{H} = \overline{\mathsf{H}} + V_{\mathrm{aspher.}}(\mathbf{r})$$

where $\overline{\mathsf{H}}$ refers to the portion containing the spherically averaged potential in region I, but the true potential in region II. We can expand the sought-for eigenstates of H in terms of the eigenstates $\psi_\lambda(\mathbf{r})$ of $\overline{\mathsf{H}}$. The asphericity-corrections $\Delta\epsilon_\lambda = \Delta\epsilon_n(\mathbf{k})$ of the band energies ϵ_λ are

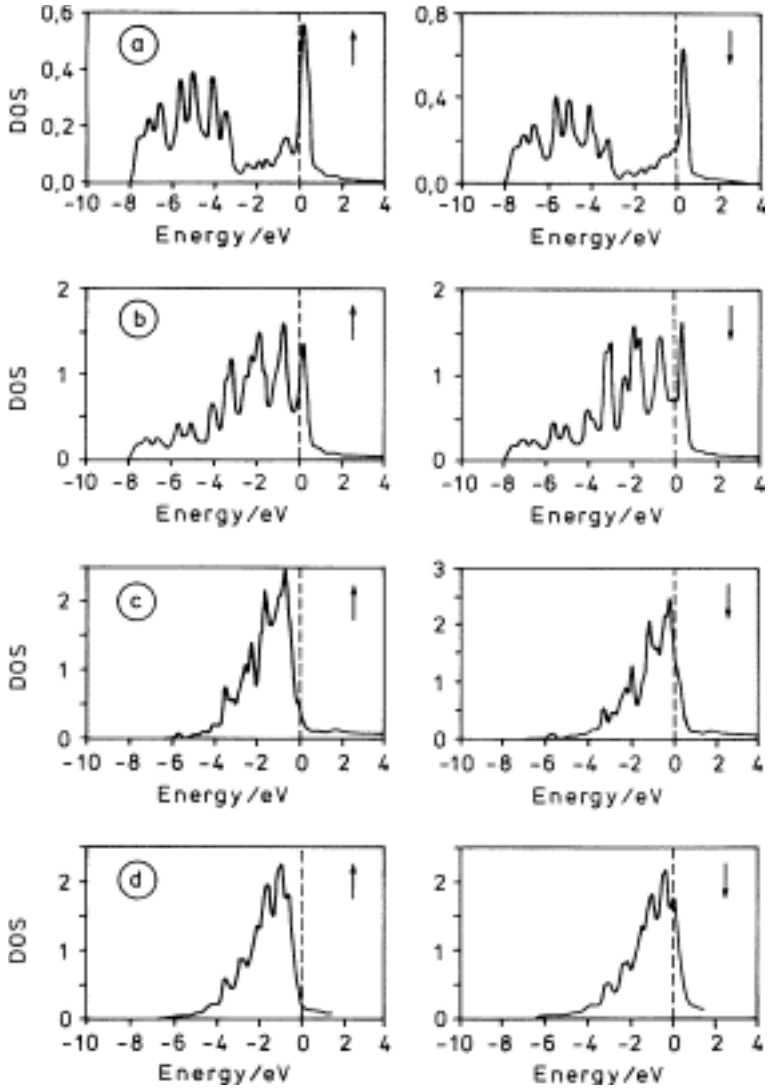

Fig. 1. Local density of states (LDOS) of a covered (Op(1 × 1)) and an uncovered 6 layer Ni(100)-film: (a) O-adlayer, (b) Ni-toplayer $Ni^{(1)}$, (c) Ni-layer opposite to O-layer $Ni^{(3)}$, (d) Ni-toplayer of uncovered 6 layer-film.

Table 6. Si band energies at special points of the Brillouin zone obtained from our scalar-relativistic FLAPW-calculations (column "a") and the respective scalar-relativistic data obtained by using the "Wien 95" code (column "b"). The experimental results are identical to those quoted by Cohen and Chelikowsky [28]. We have separately listed the non-muffin-tin corrections ("asph.pot.") that are contained in the results of a and b. All energies are given in eV.

k	asph. pot.	a	b	Exp.	
Γ	−0.052	−12.02	−11.976	−12.4 ± 0.4	Γ_1
	−0.23	0.0	0.0		$\Gamma_{25'}$
X	−0.076	−7.82	−7.83		X_1
	−0.088	−2.86	−2.86	−2.9	X_4
L	−0.075	−9.63	−9.64	−9.3 ± 0.4	L_2
	−0.044	−6.98	−7.01	−6.4 ± 0.4	L_1
	−0.154	−1.20	−1.20	−1.2 ± 0.2	$L_{3'}$

obtained then by diagonalizing the hermitian matrix

$$\mathbb{H}_{\lambda'\lambda} - \epsilon_{\lambda'}\delta_{\lambda'\lambda} \; .$$

As can be seen from Table 6, the aspherical corrections, $\Delta\epsilon_n(\mathbf{k})$, are conceivably small and only on the scale of interest for $\Gamma_{25'}$ and $L_{3'}$. In the latter case one might expect the differences in the construction of the potentials to become particularly visible if our method would suffer from a certain loss of accuracy. Obviously, the data agree very satisfactorily within the numerical accuracy which is of the order of some 10^{-2} eV.

The present study was financially supported by a grant of the German Ministry of Education and Research (BMBF).

References

1. W. Kohn, L.J. Sham, Phys. Rev. **140**, A 1133 (1965).
2. J. Harris, R.O. Jones, J. Phys. F: Metal Phys. **4**, 1170 (1974).
3. O. Gunnarsson, B.I. Lundqvist, Phys. Rev. B **13**, 4274 (1976).
4. D.C. Langreth, J.P. Perdew, Phys. Rev. B **15**, 2884 (1974).
5. L. Hedin, Phys. Rev. **139**, 1796 (1965).
6. M.S. Hybertsen, S.G. Louie, Phys. Rev. B **32**, 7005 (1985); *ibid* **34**, 5390 (1986); Phys. Rev. Lett. **58**, 1551 (1987).
7. R.W. Godby, M. Schlüter, L.J. Sham, Phys. Rev. B **37**, 10159 (1988).
8. L. Fritsche in: *Density Functional Theory*, edited by E.K.U. Gross, R.M. Dreizler, p.119 (Plenum, New York, NATO ASI Series 1995).
9. J. Cordes, L. Fritsche, Z. Phys. D **13**, 345 (1989).
10. L. Fritsche, C. Croner, T. Reinert, J. Phys. B: At. Mol. Opt. Phys. **25**, 4287 (1992).
11. O.K. Andersen, Phys. Rev. B **12**, 3060 (1975).
12. D.D. Koelling, G.O. Arbman, J. Phys. F: Metal Phys. **5**, 2041 (1975).
13. E. Wimmer, H. Krakauer, M. Weinert, A.J. Freeman, Phys. Rev. B **24**, 864 (1984).
14. M. Weinert, E. Wimmer, A.J. Freeman, Phys. Rev. B **26**, 4571 (1982).
15. C.L. Fu, A.J. Freeman, T. Oguchi, Phys. Rev. Lett. **54**, 2700 (1985).
16. H.F.J. Jansen, A.J. Freeman, Phys. Rev. B **30**, 561 (1984).
17. L.F. Mattheiss, D.R. Hamann, Phys. Rev. B **33**, 823 (1986).
18. P. Blaha, K. Schwarz, P. Sorantin, S.B. Trickey, Computer Physics Commun. **59**, 399 (1990).
19. B. Weimert, J. Noffke, L. Fritsche, Surf. Sci. **264**, 365 (1992).
20. M. Weinert, J. Math. Phys. **22**, 2433 (1981).
21. U.v. Barth, L. Hedin, J. Phys. C: Solid State Phys. **5**, 1692 (1972).
22. R.W. Godby, R. Benesh, G.A. Haydock, V. Heine, Phys. Rev. B **32**, 655 (1985).
23. R.W. Godby, Phys. Rev. B **32**, 7641 (1985).
24. J.E. Demuth, D.W. Jepsen, P.M. Marcus, Surf. Sci. **45**, 733 (1974).
25. E. Wimmer, A.J. Freeman, H. Krakauer, Phys. Rev. B **30**, 3113 (1984).
26. J.E. Demuth, D.W. Jepsen, P.M. Marcus, Phys. Rev. Lett. **31**, 540 (1973).
27. H.J. Elmers, U. Gradmann, Surf. Sci. **193**, 94-108, (1988).
28. M.L. Cohen, J.R. Chelikowsky, *Electronic Structure and Optical Properties of Semiconductors* (Berlin, Heidelberg, New York: Springer 1989).